JOURNAL OF MATERIALS SCIENCE **36** (2001) 4209–4222

Formation, faceting, and interaction behaviors of antiphase boundaries in GaAs thin films

N.-H. CHO*
Department of Materials Science and Engineering, Inha University, Inchon, Korea 402-751
E-mail: nhcho@inha.ac.kr

C. B. CARTER
Department of Chemical Engineering and Materials Science, University of Minnesota, MN, USA

Antiphase boundaries occur in GaAs epilayers grown on (001) Ge substrates by organometallic vapor-phase epitaxy methods. The formation and structural characteristics of these boundaries were investigated by transmission electron microscopy (TEM). Steps with particular heights at the surface of substrates nucleate antiphase boundaries. The observed faceting behavior of these boundaries indicates that energy associated with the presence of antiphase boundaries is strongly related with the boundary planes, and preservation of the stoichiometry of GaAs appears to play an important role in achieving a lower energy state at antiphase boundaries.

1. Introduction

Antiphase boundaries in III–V compound semiconductor materials having a sphalerite structure are of increasing technological importance because of the current interest in growing polar semiconductors on non-polar substrates. In particular, much attention has recently been focused on the use of GaAs thin films for the production of optical devices due to the direct band gap in its electronic structure. The presence of antiphase boundaries in GaAs is expected to have an important effect on the electrical properties of these materials. These interfaces currently arise in two different situations: the first is illustrated by the growth of GaAs/Ge superlattices [1, 2] and the second by the growth of GaAs-based device structures on Si [3, 4] and Ge substrates [5, 6].

The theoretical possibility that antiphase boundaries might form in materials with a sphalerite structure was noted in a report on grain boundaries in these materials [7]. Experimental evidence for their existence in GaAs was found in the early studies of the growth of GaAs on Ge substrates, in part by observing the different etching behavior of different regions of the same surface [8, 9].

These planar defects can be formed in GaAs epilayer because although it is cubic, it does not possess a crystallographic center of symmetry. When they grow on (001) Ge substrates in particular, two domains can be produced which are related to one another by inversion symmetry, i.e., the sites occupied by the Ga and As atoms in one domain are interchanged in the other. Between these two domains, a planar defect consisting of 'wrong' neighboring atoms or anti-site type bondings will form. The interface between the two antiphase domains is then conventionally known as an antiphase boundary [10]. The term used here follows the definition given by Christian, i.e., on crossing the interface "the roles of two or more sets of sites are interchanged".

Experimental TEM observations of antiphase boundaries have been reported in GaP [11]. More recently the presence of antiphase boundaries in GaAs epilayers has been observed [2, 12]. The generation of an antiphase boundary in a GaAs thin film has also been discussed [13, 14] and the crystallographic analysis and the structural behavior of antiphase boundaries in GaAs epilayers was investigated [15, 16]. Similar boundaries have been observed in SiC and in BeO [17, 18].

The energy of antiphase boundaries themselves has been discussed, and some structural considerations have suggested that the energy of antiphase boundaries depends on the plane adopted [19–21]. However, the absence of faceting of antiphase boundaries in GaP has also been reported [11]. The interaction of antiphase boundaries with line defects or planar defects can be appreciated in terms of boundary energy. In the case of antiphase boundaries in GaAs, boundary energy depends not only on general geometrical considerations but also on the number of each kind of atom present at the boundary [19].

In this study, we investigated the formation of antiphase boundaries in GaAs epilayers grown on [001] Ge substrates, the faceting phenomena of an antiphase boundary, and the interaction of antiphase boundaries with dislocations and other planar defects, such as tilt grain boundaries and interfaces in the heterostructure of GaAs/$Al_xGa_{1-x}As$ systems. Transmission electron microscopy (TEM) has been used for the structural

*Author to whom all correspondence should be addressed.

analysis. Convergent beam electron diffraction (CBED) techniques were applied to identify the antiphase boundaries [22, 23].

2. Experimental

2.1. Sample preparation

Two types of GaAs epilayers were prepared which contained antiphase boundaries. A single GaAs epilayer with a thickness of about 1.5 μm as well as a superlattice of GaAs and $Al_xGa_{1-x}As$ were grown epitaxially on (001) Ge substrates. The epilayers were grown at 650°C in a low pressure, organometallic vapor-phase epitaxy system (OMVPE). Trimethylgallium was used as the gallium source and arsine with hydrogen as the carrier gas was used to provide the arsenic.

2.2. TEM specimen preparation

Two types of transmission electron microscope specimens, namely 'flat-on' and 'cross-section' samples, were prepared for each epilayer. The flat-on type specimens were prepared in the following manner:

1. Disks of 3 mm-diameter were cut from samples.
2. These disks were mechanically polished from the Ge substrate side to a thickness of 40–50 μm.
3. These thinned disks were then milled to perforation using Ar^+ ions with an accelerating voltage of 4 kV.

Cross-section type specimens were produced in the following way:

1. The sample was cut parallel to a specific orientation.
2. The epilayers of cut samples were glued to each other, such that selected crystallographic axis of each piece was parallel.
3. These samples were mechanically polished and then ion milled in the same way as the flat-on specimens.

2.3. Imaging conditions

Examination was carried out using a JEOL 200 CX operated at 200 kV. Strong (220) two beam conditions ($s_g = \sim 0$) were applied to record images of antiphase boundaries; these reflections do not exhibit any phase shift across antiphase boundaries due to the change of polarity. Dark-field images recorded with (200) type reflections excited were used to identify the heterojunctions in $GaAs/Al_{0.3}Ga_{0.7}As/GaAs/AlAs$ heterostructure. The structure factor for these reflections indicates the difference in the atomic scattering factor between lower and higher valence atoms in III–V compound semiconductors.

To identify antiphase domains in GaAs films, CBED techniques were applied; two different types of interference between first-order Laue zone (FOLZ) reflections and (200) beams were recorded in the (200) convergent beam disks as shown in Fig. 1b. FOLZ lines are 'dark-cross' in the (200) beam disk in (a) while 'bright-cross' in (200) beam disk in (b). These two different contrasts were recorded from two domains adjoining at the antiphase boundary, shown in the bright-field image in Fig. 1, respectively with no change in the imaging conditions. Such a difference in the contrast of the high-order Laue zone (HOLZ) lines is present because there is a phase difference of π between (200) beams diffracted from one grain and the other if the two grains are antiphase-related, while for FOLZ reflection, there is little difference in phase between those from the two grains.

3. Results

3.1. Formation and annihilation of antiphase boundaries

A {220} bright-field image of antiphase boundaries is shown in Fig. 2a. The image was recorded from one of the (110) cross-section TEM specimens which were made from the heterostructure of $GaAs\text{-}Al_xGa_{1-x}As$ epilayers grown on the (001) Ge substrates. Interface between the GaAs epilayer and the Ge substrate is seen along the line indicated by an arrow between A and B; interface between GaAs and $Al_{0.3}Ga_{0.7}As$ is located along the line indicated by the arrow between layer B and Layer C. Antiphase boundaries appear as a stacking-fault-like fringe image.

Antiphase boundaries are seen to be generated right at the interface between the GaAs epilayer and the substrate. Most of the antiphase boundaries are located within a region (about one hundred nm) from the interface. The images of these antiphase boundaries appear to be of a triangular shape when the beam is parallel to the (110) direction and some of the observed antiphase boundaries propagate through the interface between GaAs and $Al_{0.3}Ga_{0.7}As$. Particular facets are observed for these antiphase boundaries. These facets are perpendicular to the interface between the epilayers and the substrates.

A (220) bright-field image shown in Fig. 2b was recorded from a (111) cross-section TEM specimen made from the GaAs epilayer grown on (001) Ge substrates. An antiphase boundary imaged as stacking-fault-like fringes is seen to propagate through the GaAs epilayer. Unlike most of the antiphase boundaries illustrated in Fig. 2a, the boundary plane of this antiphase boundary is parallel to the crystallographic plane perpendicular to the substrate when it is generated at the interface between the GaAs epilayer and the Ge substrate. This geometry can be more clearly seen from the image shown in the inset in Fig. 2b, which was recorded near the [111] pole. The image of the antiphase boundary between these two intersections shows how this boundary is generated at the interface; this antiphase boundary is shown parallel to (110) plane which is normal to the substrate.

3.2. Faceting phenomena

Fig. 3a shows a (220) dark-field image of antiphase boundaries in GaAs epilayer; this micrograph was obtained from one of the flat-on TEM specimens. Two different types of contrast appear from the antiphase boundaries. Stacking-fault-like fringes occur when

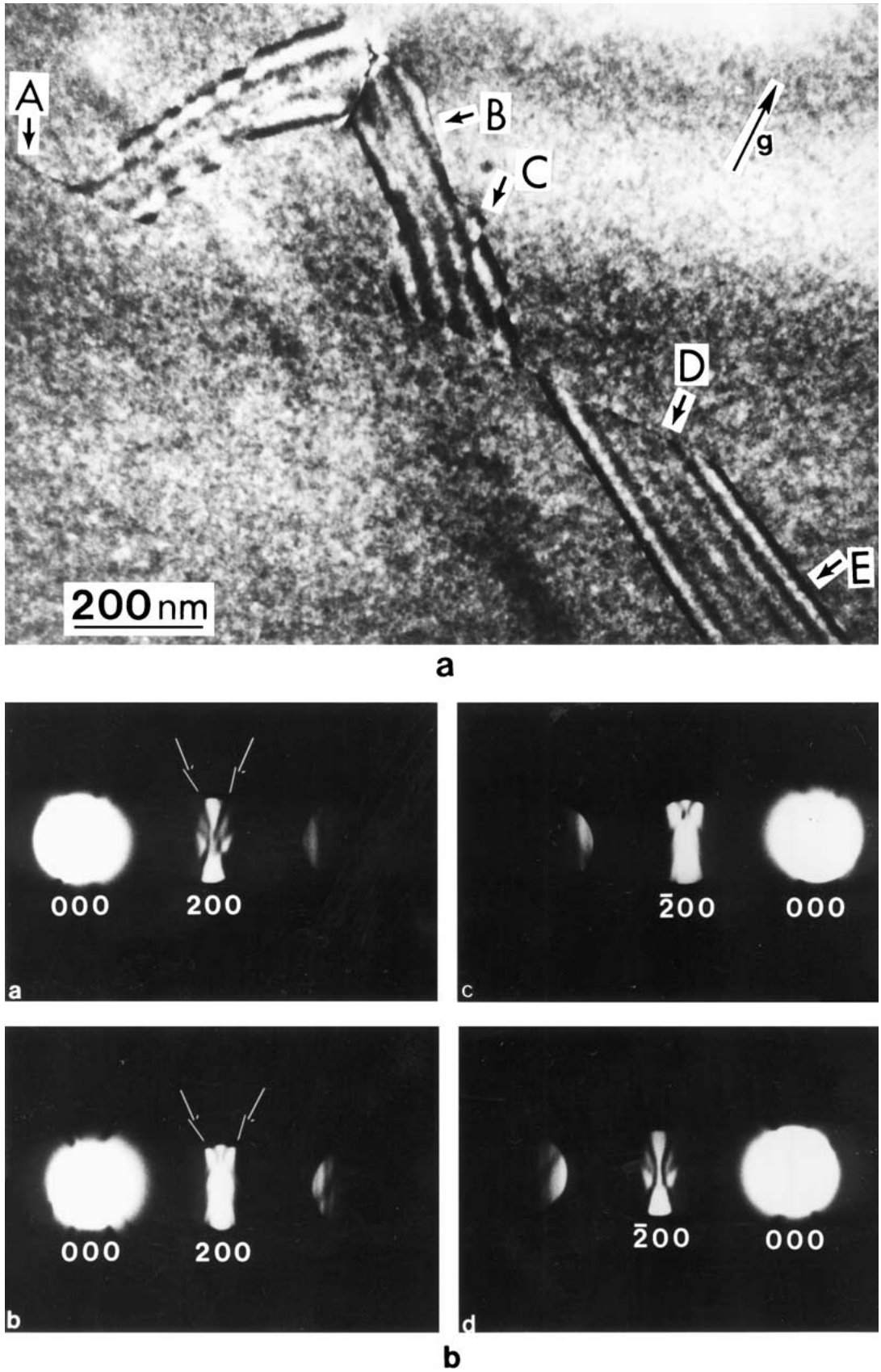

Figure 1 (a) A (220) bright-field image of an antiphase boundary. Facets are observed along the planes indicated by A-E. (b) Convergent beam electron diffraction patterns from domains on either side of the antiphase boundary shown in (a); FOLZ lines appear as a 'dark-cross' in the (200) convergent beam disk in (a) and as a 'bright-cross' in the (200) convergent beam disk in (c).

electron beams pass through antiphase boundaries, which are inclined to the surfaces, while straight lines are produced when the antiphase boundaries are lying parallel to the direction of the electron beam. The facet shown as an edge-on view in Fig. 3 is of a (110) crystallographic plane. Fig. 3b shows a selected-area diffraction pattern corresponding to the area shown in Fig. 3a. Two additional faint spots are visible close to the (220) diffraction spot in the enlarged view of the 220 reflection.

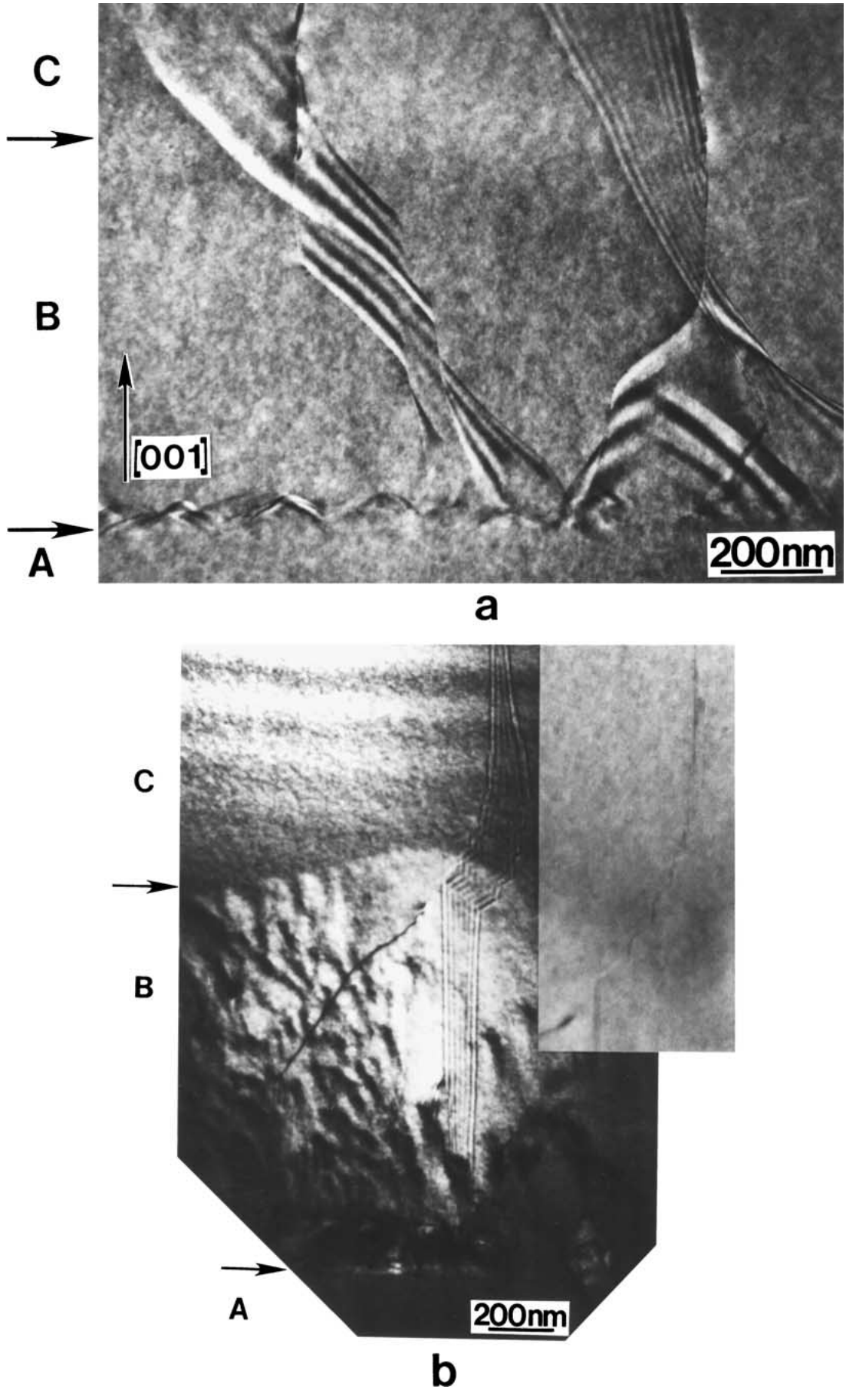

Figure 2 (a) A (220) bright-field image of antiphase boundaries in the heterostructure of GaAs-$Al_{0.3}Ga_{0.7}As$; arrow between A and B indicates interface between Ge and GaAs; arrow between B and C indicates interface between GaAs and $Al_{0.3}Ga_{0.7}As$. (b) A (220) bright-field image of antiphase boundaries; this micrograph was recorded from a (111) cross-section TEM specimen. Two arrows indicate intersections between the interface and the surfaces of specimen foil. An edge-one type image is shown for the boundaries in the inset; (110) antiphase boundaries are seen.

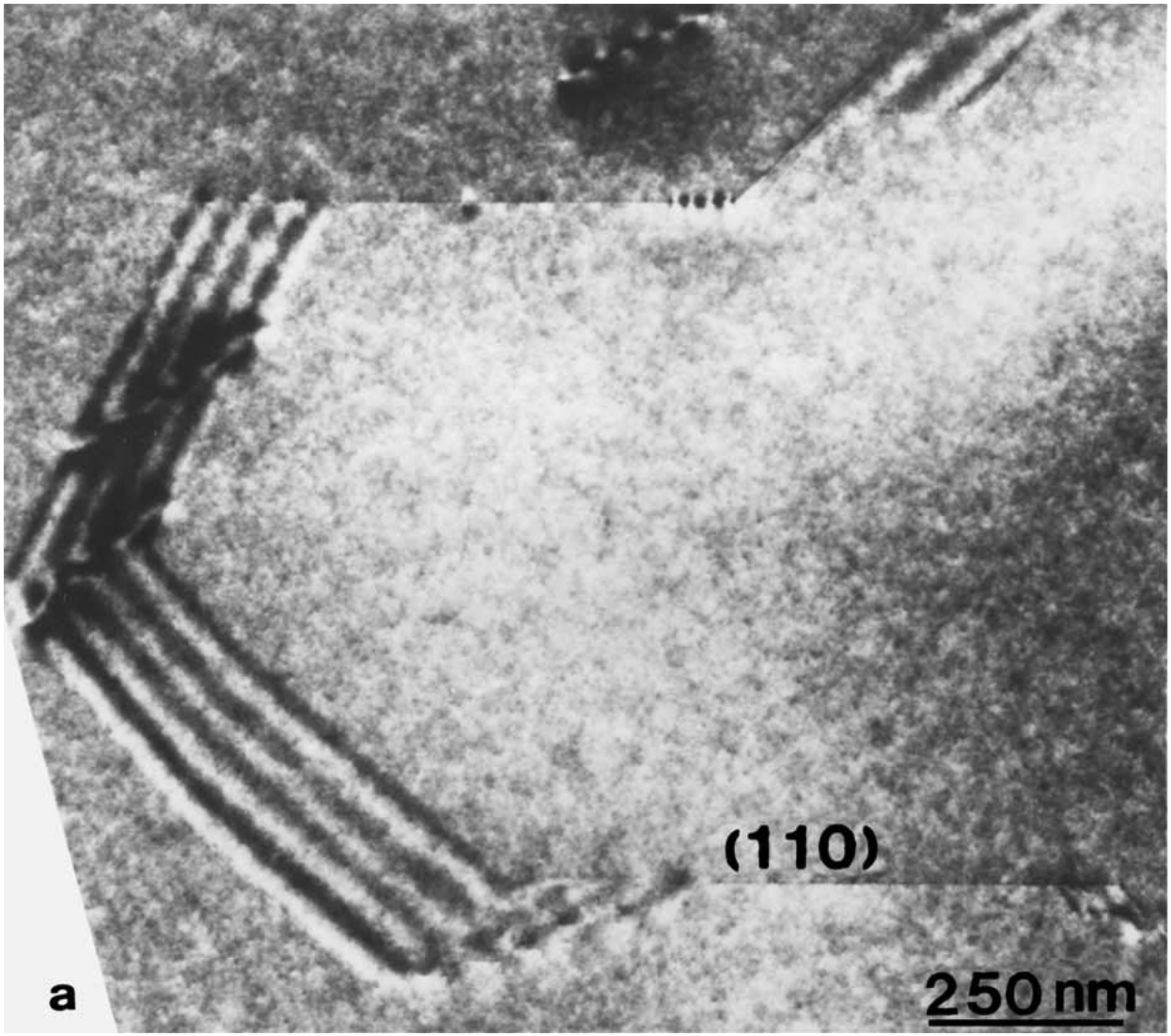

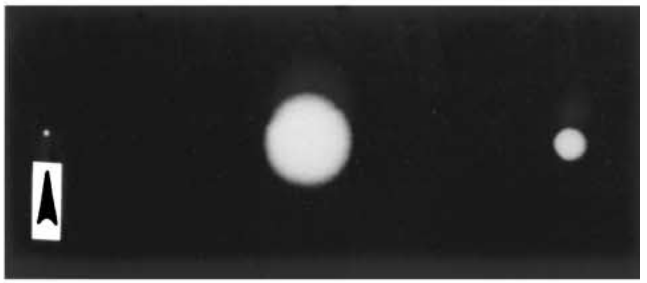

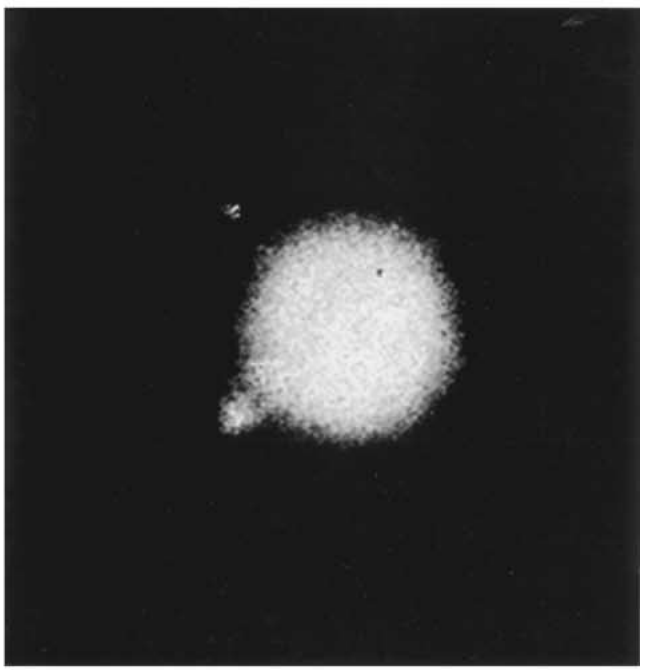

b

Figure 3 (a) A (220) dark-field image of an antiphase boundary; micrograph recorded from a flat-on specimen; facets parallel to {110} crystallographic planes are observed; stacking-fault-like fringes are seen when the boundaries are inclined to the surfaces. (b) Selected-area diffraction pattern corresponding to the antiphase boundaries inclined to the surface of the specimen.

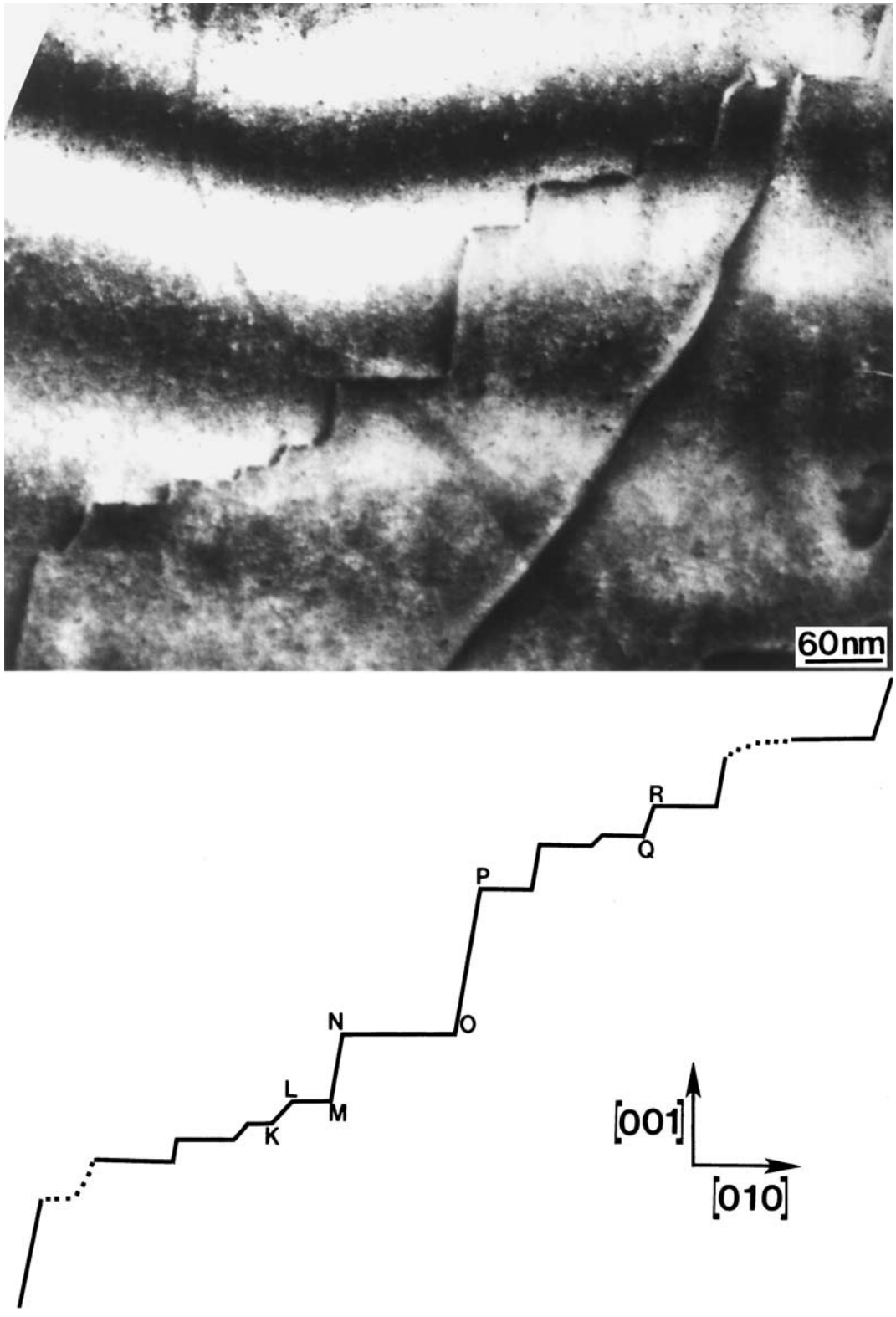

Figure 4 A (220) bright-field image of antiphase boundaries; (110), (130), (510) and (001) facets are seen at KL, QR, OP and NO, respectively.

A (220) bright-field image of a region containing several antiphase boundaries is shown in Fig. 4a; this diffraction image was obtained from the cross-section TEM specimens. Thickness fringes are seen nearly parallel to the specimen edge. Antiphase boundaries appear to facet parallel to particular planes; (100), (110), (130), and (510) facets are shown along NO, KL, OP and QR in Fig. 4b.

A (220) bright-field image of an antiphase boundary is shown in Fig. 5; this micrograph was recorded with a (220) beam excited at near [$\bar{1}$13] pole. A corresponding selected area diffraction pattern recorded near the pole is shown in Fig. 5b. The antiphase boundaries are also observed to facet parallel to ($\bar{1}2\bar{1}$) and ($\bar{2}1\bar{1}$) planes, in addition to (110) plane.

3.3. Interaction behaviors

A (220) bright-field image of an antiphase boundary is shown in Fig. 6a; the micrograph was recorded from a

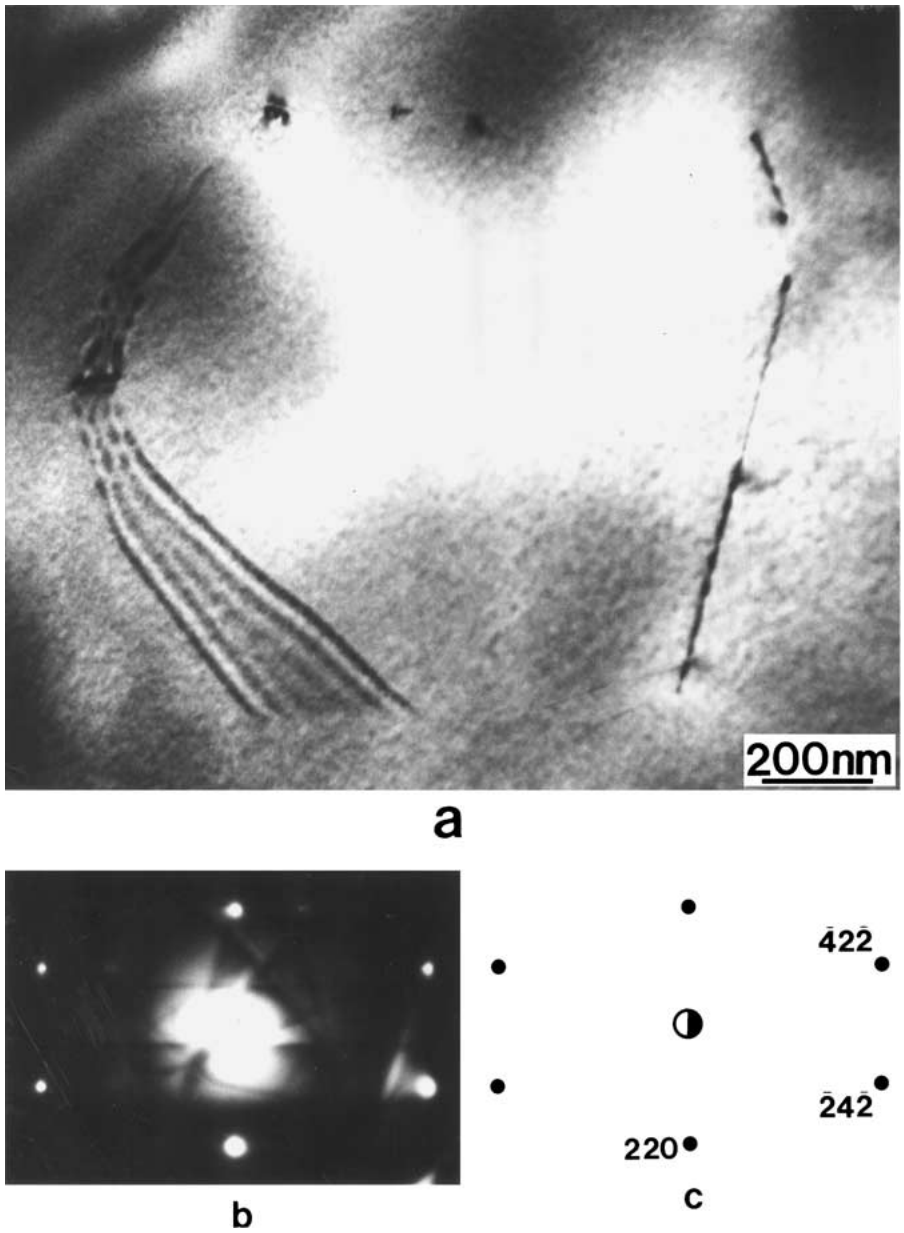

Figure 5 (a) A (220) bright-field image of antiphase boundaries; this micrograph was recorded with the direction of electron beam almost parallel to the [113] pole; facets parallel to $(\bar{2}1\bar{1})$ and $(\bar{1}2\bar{1})$ crystallographic planes are seen. (b) Selected-area diffraction pattern corresponding to the area shown in (a). (c) Schematic of the selected-area diffraction pattern shown in (b).

flat-on TEM specimen. Dislocations indicated by letter D are seen along the boundary plane; these dislocations lie between two points of the intersections between the top and bottom surfaces of TEM foil and the antiphase boundary. The image of these dislocations is typical of the dislocations interacting with antiphase boundaries inclined to the surface.

A cross-section view of the interaction of dislocations with an antiphase boundary is shown in Fig. 6b. The dislocations are seen to propagate through the GaAs epilayer. When they come across the antiphase boundary, they do not propagate through the boundary but they are seen to lie along the boundary plane.

In Fig. 7, grain A and grain B are $\Sigma = 3$-related and coherent twin boundaries are shown at KL and MN. A $\Sigma = 3$ lateral twin boundary is seen between L and M. An (110) antiphase boundary is observed along segment QL. Interaction of the antiphase boundary is seen at segment ML.

An antiphase boundary is observed to propagate through heterolayers of GaAs/$Al_{0.3}Ga_{0.7}As$/GaAs/AlAs in Fig. 8. These micrographs were recorded from a cross-section TEM specimen of heterolayers. The boundaries inclined to the foil surface also facet parallel to (110) planes. In the (200) dark field image shown in Fig. 8b, each layer is seen clearly; the structure factor of (200) reflection for GaAs is very sensitive to the difference of atomic scattering factor between Ga and As.

The interface between a GaAs layer and a $Al_{0.3}Ga_{0.7}As$ layer and the interface between AlAs layer and GaAs layer are shown to be very flat as expected. However, the presence of an antiphase boundary through the heterolayer is observed to change the position of interfaces across the antiphase boundary as shown in Fig. 8c. The position of the interface between GaAs and $Al_{0.3}Ga_{0.7}As$ is translated by about 20–30 nm at P and T, where an antiphase boundary intersects the interfaces.

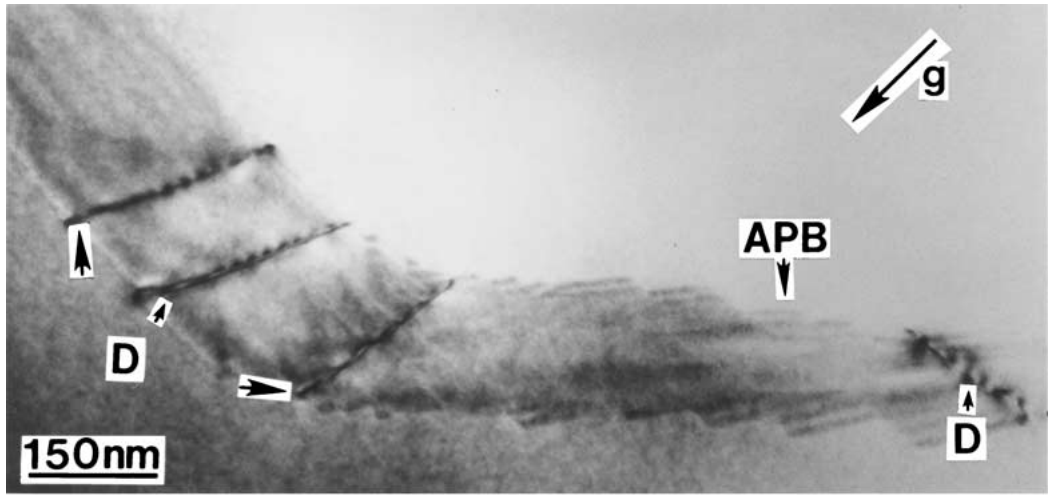

a

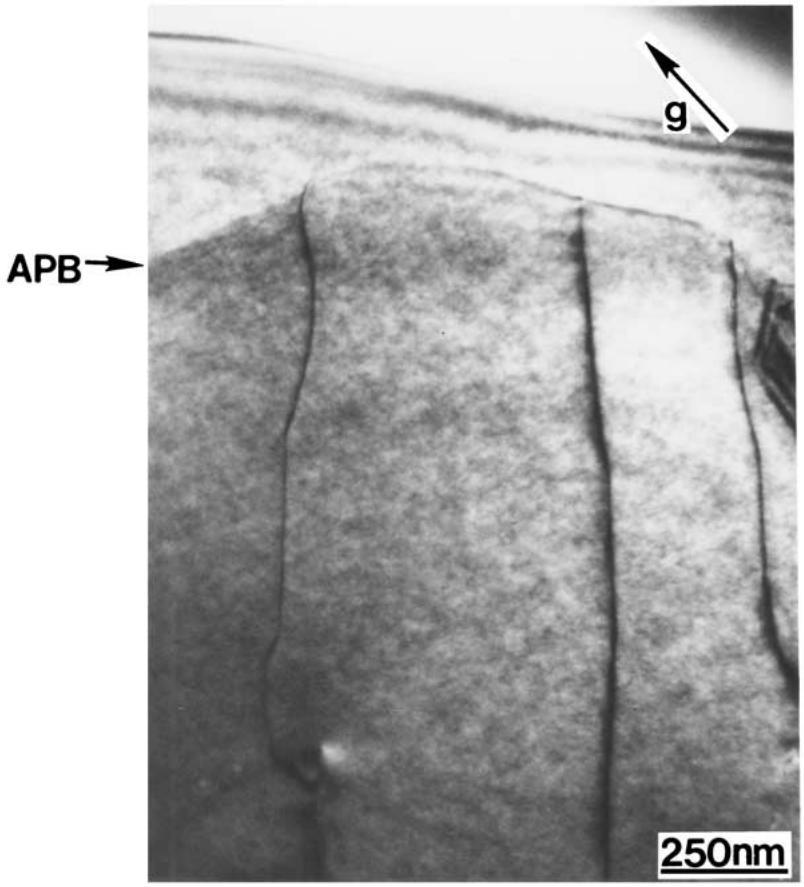

b

Figure 6 (a) A (220) bright-field image of an antiphase boundary; D indicates dislocations. (b) A (220) bright-field image of an antiphase boundary; this micrograph was recorded from a (111) cross-section specimen.

4. Discussion

4.1. Formation and annihilation of antiphase boundaries

From the observation of antiphase boundaries in GaAs epilayers grown on near (001) Ge substrates, antiphase boundaries are generated very frequently at the interface of GaAs epilayers and substrates. The formation of antiphase boundaries in GaAs epilayers is expected to be associated with the geometrical condition of (001) Ge surfaces, the atomic reconstruction at the surface of the substrates at growing temperature and the difference in affinity between Ga and As atoms to the Ge substrates in the atmosphere of the growing condition.

In the heterostructure of GaAs/(001) Ge or GaAs/(001)Si, the surface of Ge or Si substrates may first be saturated with As or with Ga, if there is little preference regarding which atom bonds to the substrate. Antiphase boundaries consisting of anti-site type bonding are produced where two grains meet one another, and when the first growing layer of each grain on either side of the boundary is different one from the other. Fig. 9 illustrates a schematic of the generation of

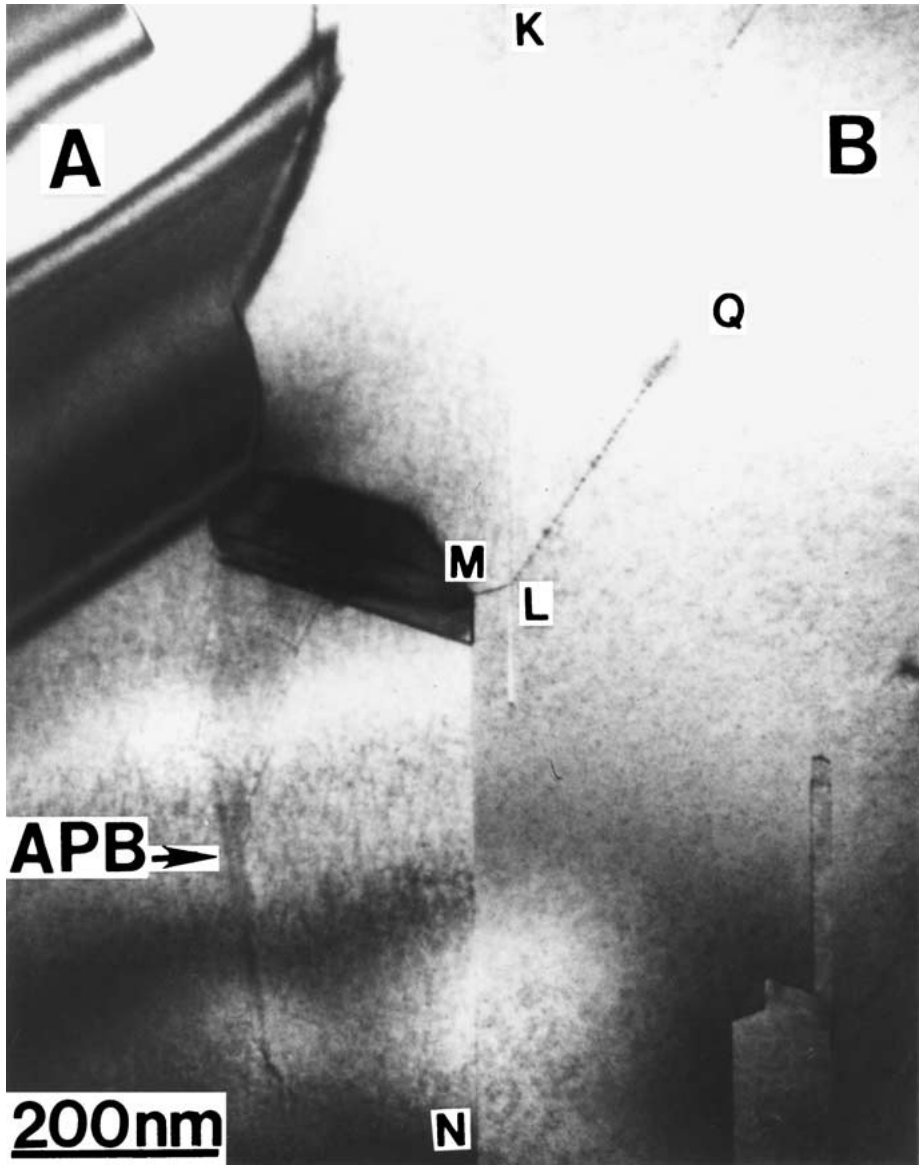

Figure 7 A bright-field image of coherent twin boundaries (KL and MN) and antiphase boundaries; a (110) antiphase boundary is seen along QL; a lateral twin boundary is observed to interact with an antiphase boundary along LM.

(110) antiphase boundaries due to the coalescence of two crystals. In this illustration, the two grains started growing with different first-layers on the (001) Ge substrate. Fig. 9b shows an atomic model of the generation of antiphase boundary in a GaAs epilayer grown on a (111) Ge substrate. The boundary is lying parallel to {112} crystallographic plane, which is perpendicular to the (111) substrate surface. Another possible generation of an antiphase boundary on (111) Ge substrates is illustrated in a schematic shown in Fig. 9c. the crystallographic plane of the antiphase boundary is of (001) and this boundary is inclined to the direction normal to the surface of the substrate unlike the boundary planes shown in Fig. 9a and b.

The other possible sources of antiphase boundary generation are schematically illustrated in Fig. 10. The schematic in Fig. 10a shows that (110) antiphase boundaries can be produced if partial surface steps with a/4[001] are present on an (001) Ge substrates, even when the Ge surface is saturated with only one kind of two atoms. This boundary is inclined to the (001) Ge substrate by 45°. In Fig. 10b, the antiphase boundary is also expected to be produced along an (110) crystallographic plane when there is a a/4[001] surface step; this boundary is perpendicular to the surface of the substrate.

Most antiphase domains in GaAs epilayers are located near the interface between GaAs epilayer and Ge substrates. Such a tendency can be explained by the presence of steps, the probable origin of antiphase boundaries, and the strong tendency to facet parallel to particular plane such as (110) type crystallographic planes. The triangular images of antiphase boundaries shown near the interfaces in Fig. 2 can support a geometrical model in which antiphase boundaries are produced where particular partial steps are present, as explained in Fig. 10, and then propagate along particular crystallographic planes such as (110) planes. When these two antiphase boundaries meet one another while propagating in their own directions, the resultant antiphase domain will stop expanding through the epilayers.

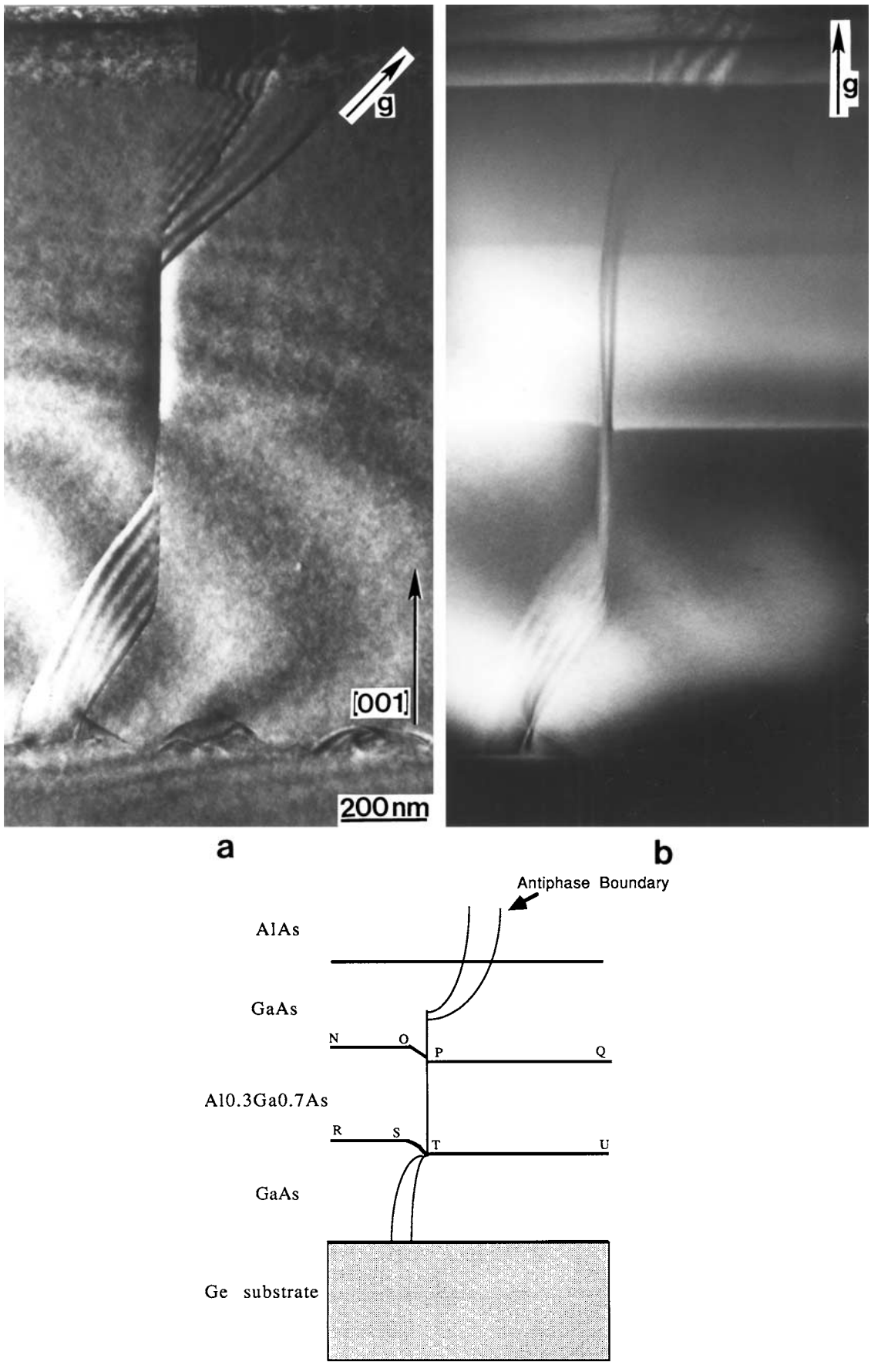

Figure 8 (a) A (220) dark-field image of antiphase boundaries; this micrograph was recorded from a cross-section specimen of the heterostructure of GaAs/$Al_{0.3}Ga_{0.7}As$/GaAs/AlAs. (b) A (200) dark-field image of the same area shown in (a). (c) A schematic of the geometry of the heterostructure.

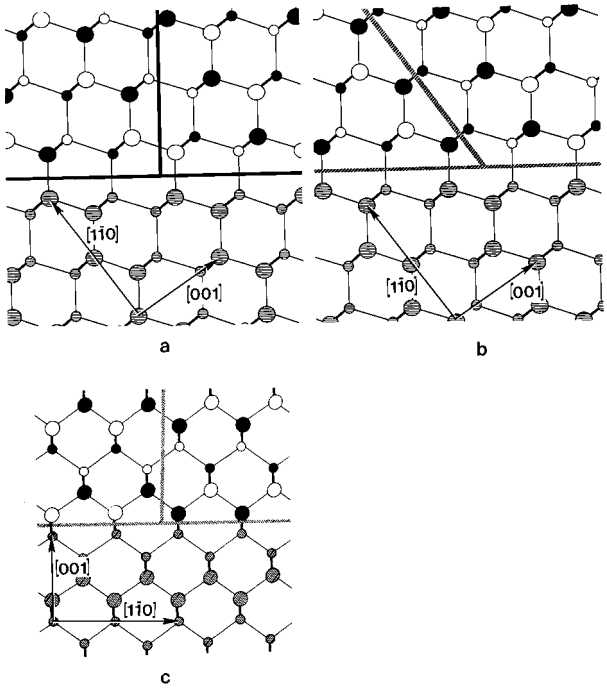

Figure 9 Geometrical consideration for formation of antiphase boundaries in polar semiconductor materials (GaAs) grown on non-polar semiconductor materials (Ge) when there is no steps at surface of substrate. Hatched circles indicate Ge atomic sites; open and closed circles indicate Ga and As atomic sites respectively or vice versa; the difference in size indicates the difference in height normal to the paper.

This annihilation of antiphase boundaries indicates that antiphase boundaries can be prevented from propagating through epilayers by locating a sufficient number of closely spaced steps of the opposite sign. These steps will then nucleate mutually inclined pairs of inclined antiphase boundaries. In the same sequence, if steps with a particular height such as 2n*a/4[001] are present at the surfaces and the first layer of epilayers is saturated with one kind of atoms, antiphase boundaries cannot be nucleated at these steps. This type of step is important since it has been found that when Ge is annealed at high temperatures, the surface steps tend to coalesce to form double steps. Such a coalescence occurs because it allows surface bond reconstruction to take place at the double steps with a subsequent lowering of the step energy.

On the other hand, the observation of the antiphase boundaries lying along crystallographic planes perpendicular to the surface of substrates at the initial stage of their propagation indicates that antiphase boundaries may also be generated due to the geometrical reason illustrated in Fig. 10.

4.2. Faceting phenomena

The image of a straight line along antiphase boundaries indicates that the boundary has a tendency to lie parallel to particular crystallographic planes. In addition, such a contrast from the boundaries results from the difference in the atomic arrangement at these boundaries from that of a perfect crystal region. The Ga-Ga and As-As antisite type bonds inherent to these boundaries give rise to both local atomic relaxation and lattice translation at boundaries.

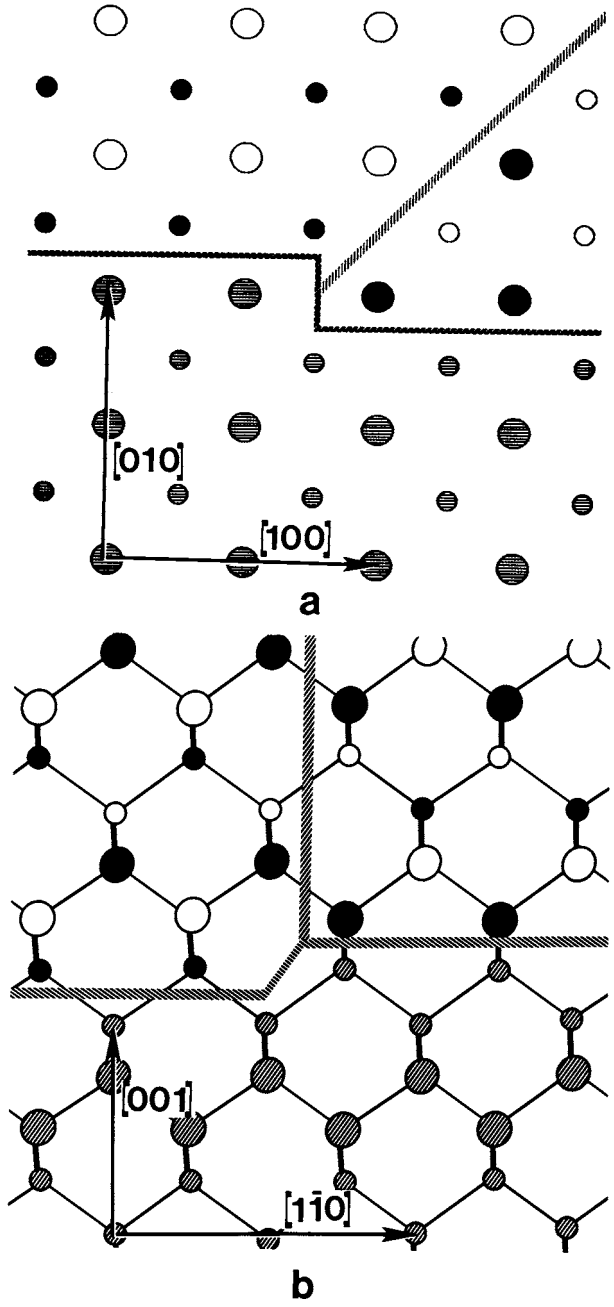

Figure 10 Geometrical consideration for formation of antiphase boundaries in polar semiconductor materials (GaAs) grown on non-polar semiconductor materials (Ge) when there are steps with particular heights.

Such a deviation from the atomic arrangement of a perfect crystal region can also be observed from the satellite spots in selected area diffraction pattern shown in Fig. 3b. The origin of these satellite spots can be understood from the geometry of reciprocal lattice of an inclined antiphase boundary. As is shown in Fig. 11, each of the matrix reflections is elongated in a direction q normal to the specimen foil plane and in directions p_1 and p_2 normal to the antiphase boundary planes; the extension of the relrods normal to the antiphase boundaries is expected to be narrower and longer than that normal to the specimen surface because the atomic structure along the antiphase boundaries are of a near two-dimensional crystal. The diffraction spots shown in Fig. 3b are produced when the Ewald sphere cuts the relrods of intensity distribution as shown in Fig. 11.

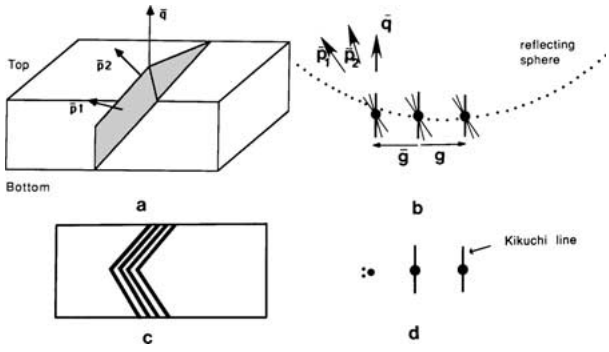

Figure 11 Geometry of diffraction from the interface illustrated in Fig. 3. (a) Antiphase boundary planes are in TEM specimen foil; q is a vector normal to the surface of foil; p1 and p2 are vectors normal to the antiphase boundary planes. (b) The Ewald sphere construction. (c) Schematic of the flat-on view of the antiphase boundaries. (d) Schematic of the diffraction pattern showing the two 'satellite' spots.

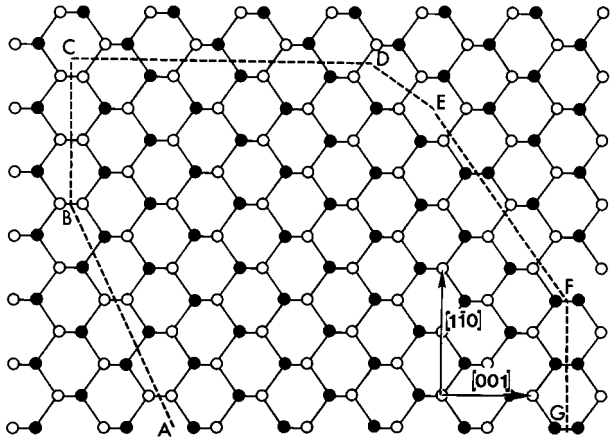

Figure 12 [110] projection of an antiphase domain surrounded by antiphase boundaries (A–G). The boundaries facet parallel to particular crystallographic planes.

The presence of such satellite spots in the selected area diffraction pattern of inclined antiphase boundaries strongly indicates that the inclined interfaces are very flat.

Antiphase boundaries can be categorized into three different groups in terms of the stoichiometry of the anti-site bonds, which are illustrated in Fig. 12. If the number of anti-site bonds across the interface is the same for both elements, the chemical composition at the boundary is stoichiometric and the interface is referred to as type A. Such an interface occurs when the facets of the antiphase boundary are parallel to a/4⟨111⟩ vector. As the segments of CD and EF in Fig. 12 illustrate, the {110} and {112} antiphase boundaries are of type A. The number of Ga-Ga bonds is the same as that of the AS-As bonds along these facets.

This stoichiometry can also be preserved at {130} and {510} antiphase boundary planes. Fig. 13 illustrates schematics of these facets on the atomic scale. A schematic of a (130) antiphase boundary is shown in Fig. 13(a). This schematic indicates that a structural unit of two Ga-Ga and two As-As anti-site bonds is repeated along this boundary and that the total number of Ga-Ga and As-As bonds is same. An atomic model of the {510} antiphase boundary plane shown in Fig. 13b illustrates that a structural unit of three Ga-Ga and three As-As

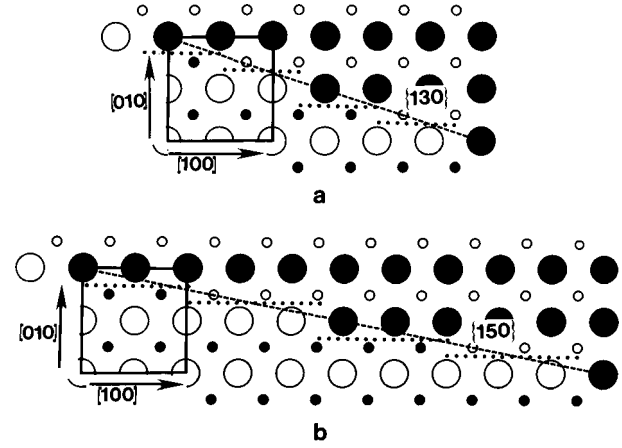

Figure 13 Schematic diagrams of (130) and (150) antiphase boundaries in the (001) projection.

anti-site bonds is arrayed along the boundary. The total number of Ga atoms is the same as that of As along this boundary plane.

If all the bonds across an antiphase boundary are of the same type, the interface is referred to as type 2. Some of the crystallographic planes belonging to this type are of a very low index plane like {100} or {111}. The {100} plane has been observed as one of the facets of antiphase boundaries shown in Fig. 4. The atomic structure of antiphase boundaries with a low-index is presumably of a lower-energy state. This state can be obtained partly because atoms form a particular structural unit with lattice translation and local atomic relaxation at the boundary, compromising the negative effect of the nonstoichiometry on the stability of the boundary. Thirdly, the interface may involve an unequal mixture of wrong bonds between these two extremes; the (130) plane involves a 2:1 ratio if this plane becomes an antiphase boundary. Boundaries belonging to the third group have not been observed in this study.

4.3. Interaction behaviors

Fig. 14 is a schematic of a TEM specimen foil with a (110) antiphase boundary plane in it; this boundary is extended and a Thomson tetrahedron is drawn to be overlapped to the specimen. A dislocation (Dl) is supposed to be generated at the interface between GaAs epilayers and Ge substrates. This threading dislocation is propagating (gliding) on a (111) slip plane, expanding the dislocation loop (D2). A segment of the dislocation (D3) encountering the antiphase boundary is trapped along the boundary. As the dislocation loop expands, the dislocation segment lying along the antiphase boundaries will be extended. Eventually, the antiphase boundaries will prohibit threading dislocations from propagating through the GaAs epilayer. When the dislocation trapped at the antiphase boundary is imaged on a flat-on view, it will be seen as is shown is Fig. 14b.

As previously discussed, and inversion symmetry exists across an antiphase boundary. The interaction of an antiphase boundary with grain boundaries changes the polarity (the relative position of Ga and As) in one grain,

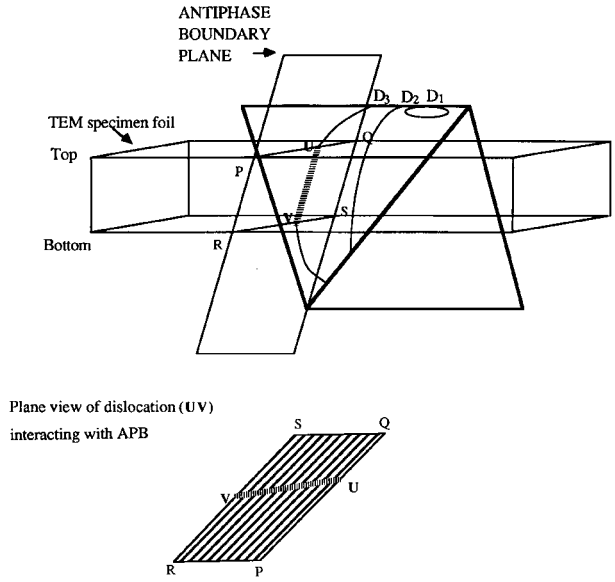

Figure 14 (a) Geometrical relationship for a particular (110) antiphase boundary and a dislocation gliding on a (111) slip plane. A dislocation loop is generated (D_1) and extends on a (111) slip plane of the Thomson tetrahedron. A portion of the dislocation (D_3) is trapped at the antiphase boundary. (b) Flat-on view of the dislocation at the antiphase boundary.

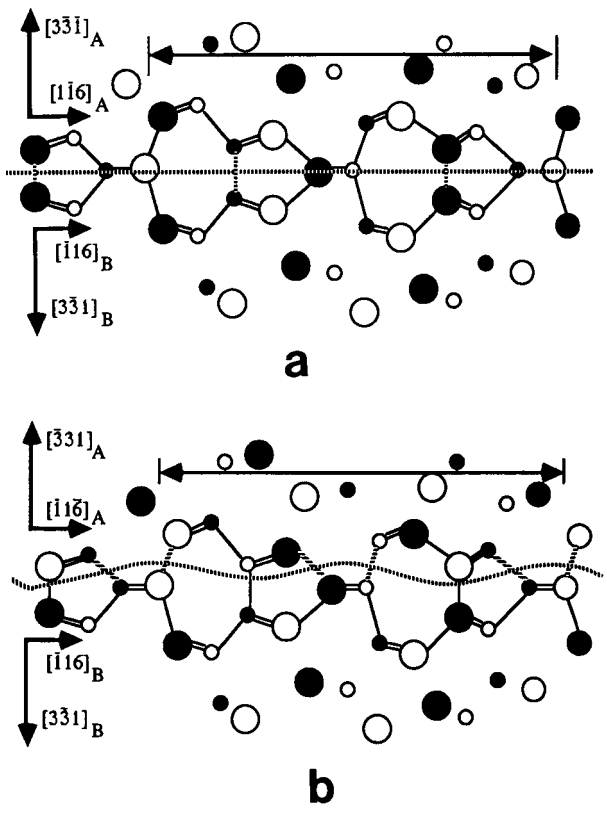

Figure 15 (a) Model of the atomic structure for a $\Sigma = 19$, $(3\bar{3}\bar{1})/(3\bar{3}1)$ [110] tilt grain boundary in GaAs. (b) Atomic structure for the same boundary shown in (a) when the polarity in the upper grain is reversed.

such that the type of bonds across the boundaries is reversed, i.e., from a normal bond to an anti-site bond, or vice versa. In Fig. 15, two atomic structures of $\Sigma = 19$, $(3\bar{3}\bar{1})/(3\bar{3}1)$ tilt grain boundaries are illustrated. The increase in the number of anti-site type bonds can be seen when the polarity in the upper grain is reversed from that of (a). The density of anti-site type cross-boundary bonds is higher in (b) than in (a). The energy associated with the presence of this tilt grain boundary is, therefore, expected to increase considerably when the boundary with the atomic structure shown in (a) interacts with an antiphase boundary having the atomic structure shown in (b).

A schematic shown in Fig. 8c illustrates the geometric relation of an antiphase boundary with the interfaces between each layer. The antiphase boundary originally produced at the interface propagates through the interfaces. This propagation indicates how the first layer of the epilayer is formed when the heterolayers are grown on top of other layers; an ordered $Al_{0.3}Ga_{0.7}$ atomic plane is saturated on top of the As plane of the GaAs epilayer and an As atomic plane is saturated on top of the Ga plane of the GaAs epilaryer. The strong tendency to form the next layer in heterostructure in this way allows an antiphase boundary to propagate through the given heterojunctions.

The difference in the position of interfaces between GaAs and $Al_{0.3}Ga_{0.7}As$ represented by NO and PQ in Fig. 8c is believed to result from the difference in the growth rate of the GaAs and $Al_{0.3}Ga_{0.7}As$ between two domains on either side of the antiphase boundary. The resultant steps are present along OP and ST. The step is bent near the corner where the two boundaries are interacting with one another. This occurs because the atoms are mobile enough to reduce the energy associated with the interface and the antiphase boundary at the corner.

5. Conclusion

Antiphase boundaries occur in GaAs epilayers grown on (001) Ge substrates by OMVPE. These boundaries have been imaged by TEM from cross-section and flat-on specimens. The comparison of the experimental images with geometrical models confirms that steps with particular heights at the surfaces of substrates nucleate antiphase boundaries, and (in reverse) these boundaries can be annihilated by the other antiphase boundaries generated at other steps.

Strong faceting phenomena observed at antiphase boundaries indicate that energy associated with the presence of antiphase boundaries is strongly related with the boundary planes. From the observation of the (110), (112), (130) and (510) boundary planes, it is believed that preservation of the stoichiometry of GaAs plays an important role in achieving a lower energy state at antiphase boundaries. The local strain field near the core of dislocations is expected to be reduced when the dislocation interacts with antiphase boundaries. Such an interaction lowers the energy state of the system containing both antiphase boundaries and dislocations.

References

1. P. M. PETROFF, A. C. GOSSARD, A. SAVAGE and W. WIEGMAN, *J. Cryst. Growth* **46** (1979) 172.
2. C. A. CHANG and T. S. KUAN, *J. Vac. Sci. Technol. B* **1** (1983) 315.
3. W. I. WANG, *Appl. Phys. Lett.* **44** (1984) 1149.
4. R. M. FLETCHER, D. K. WAGNER and J. M. BALLANTYNE, *ibid.* **44** (1984) 967.
5. H. K. CHOI, B.-Y. TSAUR, G. M. METZE, G. W. TURNER and J. C. C. FAN, *IEEE El. Dev. Lett.* **5** (1984) 207.

6. S. SAKAI, T. SOGA, M. TAKEYASU and M. UMENO, *Jpn. J. Appl. Phys.* **24** (1985) L666.
7. D. B. HOLT, *J. Phys. Chem. Solids* **23** (1962) 1353.
8. L. C. BOBB, H. HOLLOWAY, K. H. MAXWELL and E. ZIMMERMANN, *J. Appl. Phys.* **37** (966) 4687.
9. H. D. BARBER and E. L. HEASELL, *J. Phys. Chem. Solids* **26** (1965) 1561.
10. J. W. CHRISTIAN, in "The Theory of Transformations in Metals and Alloys, Part 1, Equilibrium and General Kinetic Theory," 2nd ed. (Pergamon Press, Oxford, 1977) p. 213.
11. K. MORIZANE, *J. Cryst. Growth* **38** (1977) 249.
12. N.-H. CHO, B. C. DECOOMAN and C. B. CARTER, *Appl. Phys. Lett.* **47** (1985) 879.
13. J. H. NEAVE, P. K. LARSEN, B. A. JOYCE, J. P. GOWERS and J. F. VAN DER VEEN, *J. Vac. Sci. Technol. B* **1** (1983) 668.
14. C. B. CARTER, B. C. DECOOMAN, N.-H. CHO, R. M. FLETCHER, D. K. WAGNER and J. BALLANTYNE, *Mat. Res. Soc. Symp. Proc.* **56** (1986) 73.
15. N.-H. CHO, S. MCKERNAN, C. B. CARTER and D. K. WAGNER, in Proceedings of the 45th Ann. Meeting of the EMSA (1987) p. 314.
16. C. B. CARTER, N.-H. CHO, S. MCKERNAN and D. K. WAGNER, *Mat. Res. Soc. Symp. Proc.* **91** (1987) 181.
17. H. S. KONG, Y. S. WANG, J. T. GLASS and R. F. DAVIS, *J. Mater. Res.* **3** (1988) 521.
18. J. CHIKAWA and S. B. AUSTERMAN, *J. Appl. Cryst.* **1** (1968) 165.
19. D. B. HOLT, *J. Phys. Chem. Solids* **30** (1969) 1297.
20. P. M. PETROFF, *J. Vac. Sci. Technol. B* **4** (1986) 874.
21. N.-H. CHO, B. C. DECOOMAN and C. B. CARTER, *Appl. Phys. Lett.* **47** (1985) 879.
22. J. TAFTO and J. C. SPENCE, *J. Appl. Cryst.* **15** (1982) 60.
23. B. C. DECOOMAN, Ph.D. thesis, Cornell University, 1987.

Received 12 April 2000
and accepted 13 April 2001